

RESEARCH ARTICLE

Silver dissolution and precipitation in an $\text{Na}_2\text{O}-\text{ZnO}-\text{B}_2\text{O}_3$ metallization paste glass

Lina Heuser¹  | Marianne Nofz¹  | Ralf Müller¹  | Joachim Deubener² 

¹Department 5 Materials Engineering, Federal Institute for Materials Research and Testing (BAM), Berlin, Germany

²Institute of Non-Metallic Materials, Clausthal University of Technology, Clausthal-Zellerfeld, Germany

Correspondence

Lina Heuser, Federal Institute for Materials Research and Testing (BAM), Unter den Eichen 87, 12205 Berlin, Germany.
Email: Lina.Heuser@bam.de

Abstract

Thermally stimulated interactions between silver and glass, that is, silver dissolution as Ag^+ and precipitation as Ag^0 were studied in two glass series of molar target composition $x\text{Ag}_2\text{O}-(19-x)\text{Na}_2\text{O}-28\text{ZnO}-53\text{B}_2\text{O}_3$ with $x = 0, 0.1, 0.5, 5$ and $(19\text{Na}_2\text{O}-28\text{ZnO}-53\text{B}_2\text{O}_3)+y\text{Ag}_2\text{O}$ with $y = 0.01, 0.05$. These act as model for low-melting borate glasses being part of metallization pastes. The occurrence of metallic silver precipitates in melt-quenched glass ingots demonstrated that silver dissolved only in traces (< 0.01 mol%) in the glasses. The dissolved silver was detected by means of Raman spectroscopy and energy-dispersive X-ray spectroscopy. Increasing x in the batch could not lead to a significant increase of the silver ion fraction in the glass as possible in binary silver borate glasses. In situ observation of heated AgNO_3 mixed with the base glass frit in a hot stage microscope showed that Ag^0 precipitation occurs already at the solid state. At higher temperatures, small droplets of liquid silver were found to move freely within the melt, whereas coalescence caused a stepwise increase of their size. These results contribute to the understanding of formation of silver precipitates in metallization pastes described in the literature.

KEYWORDS

batch reactions, borate, glass forming melts, glass manufacturing, Raman spectroscopy, silver metallization paste

1 | INTRODUCTION

Silver/glass metallization pastes are used for printed electrical wiring in photovoltaics, thick film technology and micro systems.¹⁻⁴ To ensure superior electrical conductivity, liquid phase sintering^{5,6} of silver metallization pastes containing small amounts of low melting glasses is assumed to proceed during firing. Although lead-containing paste glasses are still frequently used for this purpose,⁷ lead-free alternatives attract growing interest

to overcome environmental pollution and impairment of health.⁸⁻¹³ Most studies were focused on the overall paste performance rather than on the basic understanding of silver-glass interaction. Independent of the designated use, composition of glasses, morphological properties of silver powders, and applied heat treatments, nano to micro sized silver precipitates were reported in glasses being in contact to metallic silver at enhanced temperatures.^{5,14-18} Their formation was explained by dissolution of silver from the powder as ion, stabilization of these ions as

This is an open access article under the terms of the [Creative Commons Attribution](https://creativecommons.org/licenses/by/4.0/) License, which permits use, distribution and reproduction in any medium, provided the original work is properly cited.

© 2022 The Authors. International Journal of Applied Glass Science published by American Ceramics Society and Wiley Periodicals LLC.

part of the glass melt, and final reduction of the ions enabling formation of metallic precipitates. Details of these processes were not studied.

In the overarching scope and previous work,¹³ low melting alkali (Me) zinc borate glasses were derived from lead-free industrial paste glasses as models for the study of sintering. Among them, the sodium containing glass stood out of that $19\text{Me}_2\text{O}-28\text{ZnO}-53\text{B}_2\text{O}_3$ paste glass series due to its best performance with respect to silver silicon contact formation.¹³

In the light of the previous description, the present paper is focused on silver dissolution and precipitation in $19\text{Na}_2\text{O}-28\text{ZnO}-53\text{B}_2\text{O}_3$ glasses. The experiments were designed to keep the heat treatments shorter than necessary for approaching equilibrium states, because dwell times during technical applications using rapid thermal processing (RTP) are rather short, that is, in the range of seconds.^{17,19}

As well known from silicate glasses, a higher concentration of silver in the glass can be achieved by ion exchange, because the silver solubility is limited using conventional melting technique.²⁰ However, to incorporate the maximum silver ion concentration is not possible due to the process conditions starting with metallic silver and using short RTP times.

Silver dissolution requires the presence of oxygen in the melt and stabilization of the Ag^+ ions in the melt and glass network, respectively. In borate glasses, Ag^+ can behave like Me^+ , that is, compensate the negative charges of either fourfold coordinated boron or of nonbridging oxygen (NBO).^{21,22} Additionally, the charge compensation of $[\text{ZnO}_4]^{2-}$ by pairs of Ag^+ -ions was discussed by Chen et al.²³ With the aim to get information on the Ag dissolution and possible incorporation into the glass network up to one-quarter of the total sodium was replaced by silver in the series $x\text{Ag}_2\text{O}-(19-x)\text{Na}_2\text{O}-28\text{ZnO}-53\text{B}_2\text{O}_3$ with $x = 0, 0.1, 0.5, 5$ mol%. It will be shown by study of the glasses with Raman spectroscopy that only minor amounts of silver dissolve as Ag^+ and become constituents of the glass network. Additionally, energy-dispersive X-ray spectroscopy (EDX) analyses revealed that the percentage of dissolved silver depends on the sodium content in the samples. Hence, one part of the discussion will be related to the glass forming limit of silver containing borate systems, which is strongly influenced by the tendency of silver to form Ag^0 atoms instead of Ag^+ ions in sodium containing borate glass melts.²⁴

A second part of the work is directed to the in situ observation and thus phenomenological description of formation and growth of silver particles and droplets developing in the result of reduction of Ag^+ ions during heat treatments. Thus, in a second series, silver was added as nitrate to the base glass according to $(19\text{Na}_2\text{O}-28\text{ZnO}-53\text{B}_2\text{O}_3)+y\text{Ag}_2\text{O}$ with $y = 0.01, 0.05$ mol%.

2 | EXPERIMENTAL PROCEDURES

2.1 | Glass preparation

All glasses were prepared from Na_2CO_3 (Ensure ISO ≥ 99.9 , Merck KGaA, Darmstadt, Germany), ZnO ($\geq 99\%$, Carl Roth GmbH, Karlsruhe, Germany), AgNO_3 (99%, Chempur, Karlsruhe, Germany), and B_2O_3 (99%, Alfa Aesar/Thermo Fisher (Kandel) GmbH, Kandel, Germany). Glasses of molar target compositions $x\text{Ag}_2\text{O}-(19-x)\text{Na}_2\text{O}-28\text{ZnO}-53\text{B}_2\text{O}_3$ with $x = 0, 0.1, 0.5, 5$ (series 1) and $(19\text{Na}_2\text{O}-28\text{ZnO}-53\text{B}_2\text{O}_3)+y\text{Ag}_2\text{O}$ with $y = 0.01, 0.05$ (series 2) were obtained by different melt-quenching routines. Table 1 lists all details.

The silver-free base glass, $19\text{Na}_2\text{O}-28\text{ZnO}-53\text{B}_2\text{O}_3$ (NZN), was melted from a 3500 g batch in an inductively heated furnace (Ema Tec 2002, EMA Tec GmbH, Sonderhausen, Germany) at 1100°C for 1 h in a Pt/Rh crucible. For homogenization and due to strong crystallization tendency, the glass melt was first fritted in water and then remelted. The melt was casted onto steel molds, heated to 490°C , and cooled to room temperature without dwell time in the switched-off muffle. Thus, a bulk sample for Raman spectroscopy and a frit for preparation of samples of series 2 were obtained. The glasses $\text{Ag}0.5\text{NZN}$ and $\text{Ag}5\text{NZN}$ were produced from 15 g batches in a high-temperature laboratory furnace VMK1800 (Linn High Therm GmbH, Eschenfelden, Germany) at 1100°C for 1 h in Al_2O_3 -crucibles. These melts were immediately casted and cooled as explained for NZN. The glasses, $\text{Ag}0.01\text{NZN-H}$, $\text{Ag}0.05\text{NZN-H}$, and $\text{Ag}0.1\text{NZN-H}$, and a second charge of $\text{Ag}5\text{NZN}$ (i.e., $\text{Ag}5\text{NZN-H}$) were directly melted in the hot-stage microscope (HSM) used for the in situ observation of silver precipitation. Small Al_2O_3 -crucibles (\sim outer diameter = 5 mm, height = 2.5 mm) were used for these experiments. For $\text{Ag}0.1\text{NZN-H}$ and $\text{Ag}5\text{NZN-H}$ glasses, batches of 10 g were mixed from AgNO_3 , Na_2CO_3 , ZnO , and B_2O_3 and homogenized. About 0.01 g of these batches were poured into Al_2O_3 -crucibles. Prior to melting and HSM, the glass batches were heated to 710°C about 30 min to enable decarbonization of Na_2CO_3 and thus prevent foaming in the HSM. For $\text{Ag}0.01\text{NZN-H}$ and $\text{Ag}0.05\text{NZN-H}$, NZN-frits and water-based 0.05% AgNO_3 solution were mixed in Al_2O_3 -crucibles and dried. This technique was used to enable a homogeneous silver distribution at these low concentrations.

The chemical compositions of NZN, $\text{Ag}0.5\text{NZN}$, and $\text{Ag}5\text{NZN}$ were analyzed by inductively coupled plasma-optical emission spectrometry (ICP-OES 5100, Agilent Technologies, Waldbronn, Germany) on the basis of DIN 51086-2.²⁵ The analyzed glass composition (mol%) of NZN amounts to $19.9\text{Na}_2\text{O}-26.4\text{ZnO}-53.7\text{B}_2\text{O}_3$ being thus close to the target composition.²⁶ Parts of $\text{Ag}0.5\text{NZN}$ and $\text{Ag}5\text{NZN}$ samples were analyzed where no metallic

TABLE 1 Target glass composition (mol%), batch size (g), crucible material, and the experiments made on each glass

Glass	Ag ₂ O	Na ₂ O	ZnO	B ₂ O ₃	Batch size	Crucible material	Experiments
Series 1, furnace							
NZB	0.00	19.00	28.00	53.00	3500	Pt/Rh	ICP-OES, Raman
Ag0.5NZB	0.50	18.50	28.00	53.00	15	Al ₂ O ₃	ICP-OES, Raman, EDX
Ag5NZB	5.00	14.00	28.00	53.00	15	Al ₂ O ₃	ICP-OES, Raman, EDX
Series 1, hot-stage microscope							
Ag0.1NZB-H	0.10	18.90	28.00	53.00	0.01	Al ₂ O ₃	In situ observation
Ag5NZB-H	5.00	14.00	28.00	53.00	.01	Al ₂ O ₃	In situ observation
Series 2, hot-stage microscope							
Ag0.01NZB-H	0.01	19.00	28.00	52.99	0.01	Al ₂ O ₃	In situ observation
Ag0.05NZB-H	0.05	18.99	27.99	52.97	0.01	Al ₂ O ₃	In situ observation

Abbreviations: EDX, energy-dispersive X-ray spectroscopy; ICP-OES, inductively coupled plasma-optical emission spectrometry.

silver precipitates were visible. Their chemical analyses were not representative due to the formation of fuliginous depositions during the digestion of the samples. These can be explained by the presence of small amounts of silver as clusters or precipitates inhomogeneously distributed in the glass samples not visible with the naked eye. Due to the small amounts, the chemical compositions of the samples prepared in the HSM could not be measured.

2.2 | Raman spectroscopy

To study the effect of dissolved silver on glass structure, Raman spectroscopy was performed on fire polished bulk NZB, Ag0.5NZB, and Ag5NZB glass samples. Spectra were taken from sites where no visible silver droplets were precipitated. Raman spectra were measured from 59 to 2360 cm⁻¹ with a LabRAM HR 800 instrument (Horiba132 Jobin Yvon, Bensheim, Germany) coupled to an optical microscope (BX41, Olympus, Tokyo, Japan). The spectral resolution was 2 cm⁻¹. A quartz standard was used for wave number calibration. The laser wavelength was 633 nm with ~9 mW laser power, and a grating with 300 grooves per mm was utilized. A 50x/N.A. = 0.55 long working distance objective lens was employed for excitation and collection. For each sample, spectra were gathered from five different sites. At each site, two spectra were recorded with a measuring time of 30 s averaged to one spectrum. The spectra were baseline corrected with the software Origin 2020²⁷ using a Bspline baseline according to Wang et al.²⁸ After baseline correction, the spectra were normalized in intensity. In the range between 580 and 1050 cm⁻¹, the peaks were fitted with Lorentz alignment according to Schmid et al.²⁹

2.3 | Energy-dispersive X-ray spectroscopy (EDX)

A scanning electron microscope (Tescan Vega 3 XLH, Brno, Czech Republic) operated at 20 keV (tungsten emitter) and equipped with EDX analyzer (X-Max 80 SDD-detector, Oxford Instruments, Abingdon, UK) was used to estimate the actual amount of dissolved silver in Ag0.5NZB and Ag5NZB glasses. For normalization, the silver-to-zinc peak area ratio of the Zn-peak at 8.63 keV and the Ag-peak at 2.98 keV was analyzed by software Origin 2020.²⁷ EDX intensities were collected at three different positions of fire-polished and carbon-coated sample surfaces, where no silver droplets were detectable.

2.4 | Hot-stage microscopy (HSM)

Reflected light in situ observations of glass melting and silver precipitation were made with an HSM Metallux 3 combined with a chilled heating stage 1173 (both Leitz, Wetzlar, Germany) and a camera ProgRes Gryphax Kapella (Jenoptik, Jena, Germany). Temperature calibration was performed using 99.999% gold wires with melting temperature 1064°C. Temperatures were measured at three points in two height levels inside the Al₂O₃-crucible. The maximum temperature deviation was about ±20 K in the vertical direction and about ±5 K in the horizontal direction. The view field of the lens covered about one fifth of the 5 mm crucible diameter.

The samples were heated at 10 K/min up to 650°C and then at 5 K/min up to the observation temperatures indicated in Figure 1. The observation time was about 1 h, and the samples were cooled with 45 K/min to 440°C and

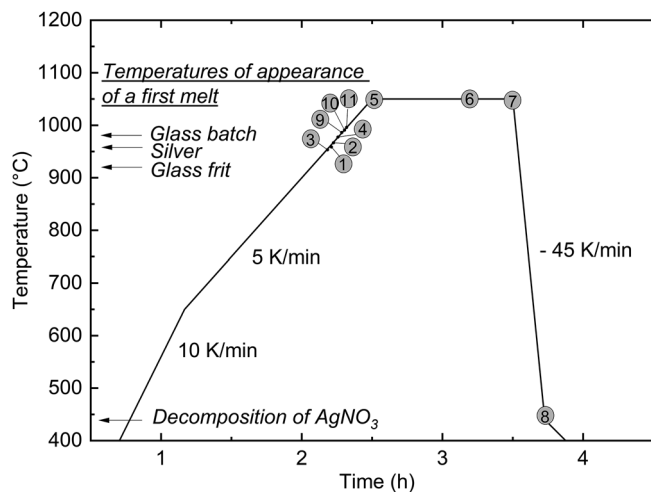


FIGURE 1 Temperature–time diagram of the hot-stage microscopy experiments. Numbers refer to Figures 4–7. Arrows indicate characteristic temperatures. Data of decomposition of AgNO_3 and melting of silver were taken from Refs. [30–32]

5 K/min to room temperature. All experiments were documented by taking videos during heating, dwelling, and cooling. Figure 1 shows the applied annealing procedure, characteristic temperatures, and the time from which the photographs shown in Figures 4–7 were taken. Temperatures of the decomposition of AgNO_3 and melting of silver were taken from Refs. [30–32]. Experiments were repeated several times to enable suitable images of the characteristic processes. All experiments were recorded with the video camera mentioned before.

3 | RESULTS

3.1 | Imaging and EDX spectroscopy

Visible silver droplet precipitation in casted $\text{Ag}0.5\text{N}Z\text{B}$ and $\text{Ag}5\text{N}Z\text{B}$ ingots clearly indicated that much less silver than batched was dissolvable into the paste glass (Figure 2). Consistently, silver droplets were found to be larger in $\text{Ag}5\text{N}Z\text{B}$ than in $\text{Ag}0.5\text{N}Z\text{B}$.

EDX spectra of the glass matrix comprised only a weak silver peak at ~ 3 keV (Figure 3), which confirmed the shortage of dissolved Ag^+ in both glasses. However, judging from the intensity ratio, dissolution was more pronounced in $\text{Ag}5\text{N}Z\text{B}$. As boron cannot be detected with standard window-based EDX analyzers, the relative amount of dissolved silver was approximated from the Ag/Zn peak area ratio. This ratio was two to three times larger for $\text{Ag}5\text{N}Z\text{B}$ (~ 0.19) than for $\text{Ag}0.5\text{N}Z\text{B}$ (~ 0.08).

3.2 | Hot-stage microscopy (HSM)

Mixtures of glass frits with silver nitrate solution yielded irregularly shaped Ag -particles upon heating to 960°C (Figure 4). Due to convection and suitable viscosity (see Section 4.2) of the matrix, the Ag -particles changed their position and liquified when exceeding the melting point at 961.9°C .^{31,32}

Larger particles were found in compositions with higher silver concentrations. Heating the $\text{Ag}5\text{N}Z\text{B-H}$ glass batch led to the complete liquification of the borate melt above $\sim 975^\circ\text{C}$. Silver aggregates melted into droplets with no change of its size, shape, and position during further dwelling for 40 min (Figure 5).

A similar observation was made in the case of the $\text{Ag}0.1\text{N}Z\text{B-H}$ composition when melted from a raw material batch in the HSM crucible. Droplets of liquid silver with size in the range $30\text{--}100\ \mu\text{m}$ did not change their lateral and horizontal positions after soaking for 1 h at 1046°C and subsequent cooling to 436°C . In addition, no steady growth of the droplet diameter was detectable during dwelling (Figure 6).

It is assumed that larger silver droplets formed stepwise through coalescence of smaller droplets during heating at temperatures $> 975^\circ\text{C}$. Figure 7 shows three single frames of a video sequence (Supporting Information section) capturing this process in the $\text{Ag}0.01\text{N}Z\text{B-H}$ melt. Two silver droplets (orange arrows) moved independently within the melt, came close to each other, and finally merged to a single silver drop. The drop diameter hereby increased from $\sim 10\ \mu\text{m}$ (Figure 7 (9) and (10)) to $12\ \mu\text{m}$ (Figure 7 (11)).

To sum up these results, it can be stated that metallic silver was precipitated in all samples (batch or frit) in the solid state, even for the glasses with the lowest nominal silver contents, $\text{Ag}0.01\text{N}Z\text{B-H}$ and $\text{Ag}0.05\text{N}Z\text{B-H}$. The precipitated Ag^0 droplets are larger in $\text{Ag}5\text{N}Z\text{B-H}$ and $\text{Ag}0.1\text{N}Z\text{B-H}$ than in $\text{Ag}0.05\text{N}Z\text{B-H}$ and in $\text{Ag}0.01\text{N}Z\text{B-H}$ due to higher fractions of silver nitrate added to the glass batch and probable more frequent coalescence of smaller droplets.

3.3 | Raman spectroscopy

Although Raman spectra appear similar at a first glance, Figure 8 indicates structural differences among $\text{N}Z\text{B}$, $\text{Ag}0.5\text{N}Z\text{B}$, and $\text{Ag}5\text{N}Z\text{B}$. The band at $937\ \text{cm}^{-1}$ decreases from $\text{N}Z\text{B}$ to $\text{Ag}5\text{N}Z\text{B}$, and a new shoulder appears for $\text{Ag}5\text{N}Z\text{B}$ at $796\ \text{cm}^{-1}$ (cyan arrow). These differences mainly result from the reduced network modifier content, as Na^+ in the batch was replaced by Ag^+ , mostly precipitating as metallic silver. Only the very weak band at $235\ \text{cm}^{-1}$ (gray arrow) in $\text{Ag}5\text{N}Z\text{B}$,

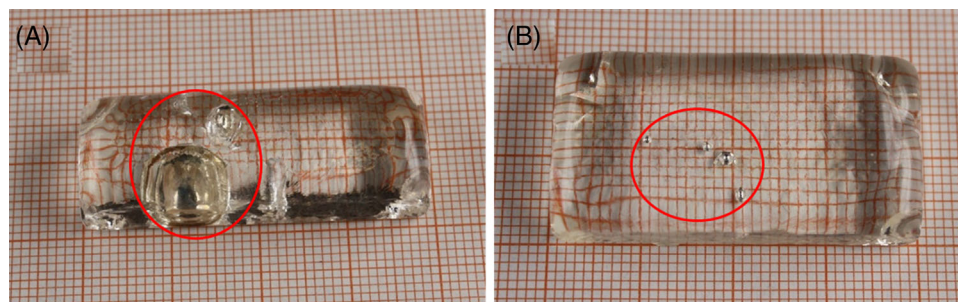


FIGURE 2 Casted and cooled ingots (size $\approx 40 \times 20 \times 5 \text{ mm}^3$) contained clearly visible silver droplets within the red ellipse (A) Ag5NZB glass (Ag droplet size $> 3 \text{ mm}$); (B) Ag0.5NZB glass (Ag droplet size $\approx 1 \text{ mm}$)

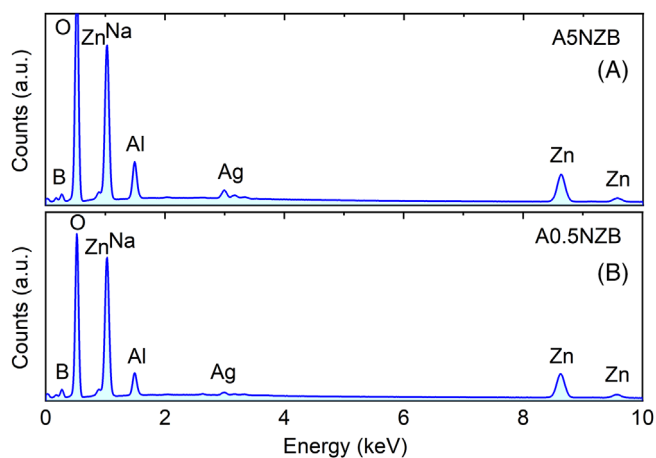


FIGURE 3 Energy-dispersive X-ray spectroscopy (EDX) spectra of (A) Ag5NZB and (B) Ag0.5NZB glasses. Note that the aluminum (Al) signal originated from a contamination of the crucible material (Al_2O_3) used for glass preparation

attributed to Ag–O vibrations,³³ proves minimum Ag^+ dissolution.

The weak bands at $280\text{--}350 \text{ cm}^{-1}$ comprise the region of vibrations of Zn–O in tetrahedral ZnO_4 ,^{34,35} metaborate,³⁶ and fourfold coordinated $[\text{B}\emptyset_2\text{O}_2]^{3-}$ units,³⁷ where \emptyset and O denote bridging oxygens and NBOs, respectively. The broad band at 445 cm^{-1} reveals metaborate units^{37,38} or “loose” $[\text{B}\emptyset_4]^-$ tetrahedral.^{37,39} Bands observed here at $\sim 540 \text{ cm}^{-1}$ can be assigned to $[\text{B}\emptyset_4]^-$ -groups^{36,37,40} and will be shown to belong to pentaborate later. The bands at $640, 730 \text{ cm}^{-1}$ (NZB) or 721 cm^{-1} (Ag5NZB), and 970 cm^{-1} can be attributed to metaborate units in rings or chains.^{37–39,41} The band at 796 cm^{-1} in Ag5NZB can be assigned to boroxol rings and only appears in Ag5NZB.^{37–39,41} The band at 852 cm^{-1} (Ag5NZB) or 843 cm^{-1} (NZB) indicates pyroborate.^{37,39,41}

The most intense band at $771\text{--}774 \text{ cm}^{-1}$ is known to be caused by six-membered $\text{B}\emptyset_3$ -rings with one $\text{B}\emptyset_3$ replaced by a $[\text{B}\emptyset_4]^-$ -tetrahedron.^{37,39} The bands at 770 and 890 cm^{-1} are assigned to rings with one

$[\text{B}\emptyset_4]^-$ -tetrahedron as parts of penta-, tri-, and tetraborate groups.^{42–44} A band at 667 cm^{-1} was interpreted as clear indication of rings with one $[\text{B}\emptyset_4]^-$ -tetrahedron as part of pentaborate groups.⁴² Due to the presence of bands at 676 or 679 and 873 or 889 cm^{-1} for NZB or Ag5NZB, respectively, the presence of $[\text{B}\emptyset_4]^-$ -units as part of pentaborate can be concluded. These can also explain the band at 540 cm^{-1} mentioned earlier. The band at 937 cm^{-1} indicates $[\text{B}\emptyset_4]^-$ -groups that cannot be further specified.^{36,37,40}

The broad band $>1000 \text{ cm}^{-1}$ is assigned to NBOs in a large borate network as described previously.^{42,45} B–O[−] stretching vibrations in metaborate $[\text{B}\emptyset_2\text{O}]^-$ -triangles in chains and rings should contribute to the band at 1421 cm^{-1} .^{37,39,41} Pyroborate units are related to the band at $\sim 1246 \text{ cm}^{-1}$.³⁷

4 | DISCUSSION

4.1 | Silver dissolution and glass structure

In general, silver dissolution is linked with the formation of Ag^+ ions balancing the charge of tetrahedral boron and/or saturating the charge of NBOs in the glass structure. Figure 9 indicates compositional trends of glass formation in the pseudoternary $\text{Ag}_2\text{O}-(\text{Na}_2\text{O}+\text{ZnO})-\text{B}_2\text{O}_3$ system, which raised undue expectations of a high silver content (up to 10 mol%) in the AgNZB glasses studied.

In the pioneer work of Boulous and Kreidl²¹, binary $\text{Ag}_2\text{O}-\text{B}_2\text{O}_3$ glasses with up to 35 mol% Ag_2O in the batch were prepared. They showed that the precipitation of nanosized silver, leading to coloration of the glasses, limits glass formation on the Ag_2O -rich side. Under the condition of the applied melt-quenching method (heating rate, glass volume), this limit was found close to 25 mol% Ag_2O . Piguet and Shelby⁴⁶ confirmed glass formation of silver borate glasses up to 30 mol% and coloration due to less than 50 ppm silver colloids.

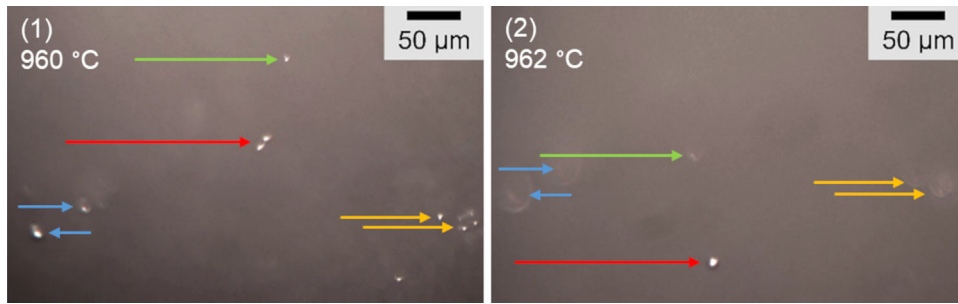


FIGURE 4 Ag_{0.05}NZB-H glass melt observed in a hot-stage microscope during heating at 5 K/min between 960°C (1) and 962°C (2). A longish silver particle (red arrow) showing two light reflections melts into a spherical drop (single reflection) and moves to a lateral position at the bottom of the figure, whereas other particles (green, orange, and blue arrows) became more diffuse. This is due to keeping the focus on the particle marked by red arrow and relative motion of the particles to each other

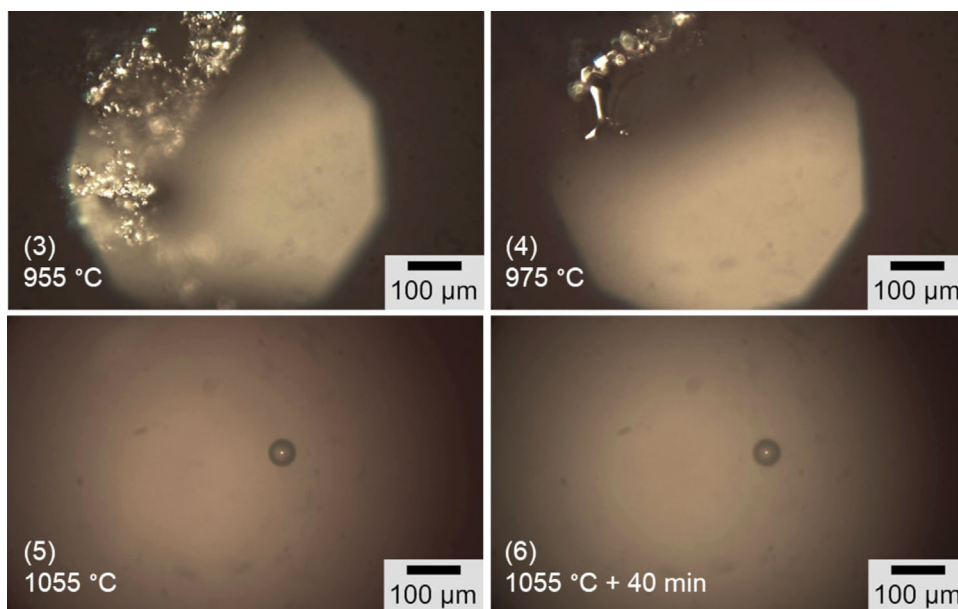


FIGURE 5 Residues of the batch with partially liquified borate melt (3) and short before complete liquification of the matrix (4) as well as development of a liquid silver droplet during ramping (5) of Ag₅NZB-H glass batch at 5 K/min to 1055°C and dwelling at this temperature for 40 min (6). In contrast to the smaller droplets of Figure 4, the droplet (diameter \approx 53 μ m) of part (5) stayed at its position during dwelling

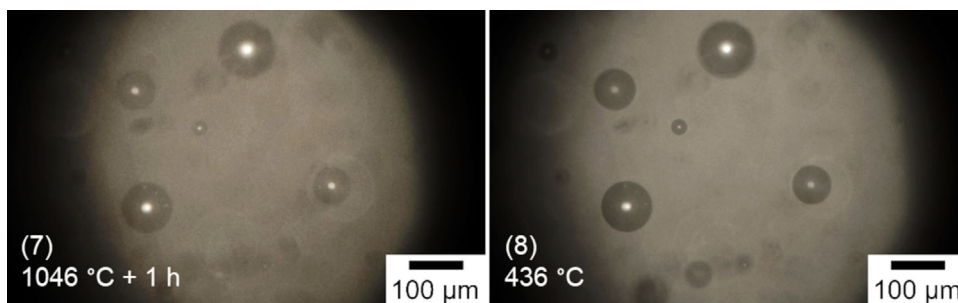


FIGURE 6 Liquid silver droplets in the Ag_{0.1}NZB-H glass melt at 1046°C after 1 h dwell time (7) and after cooling down to 436°C with 45 K/min in the hot-stage microscope (HSM) (8)

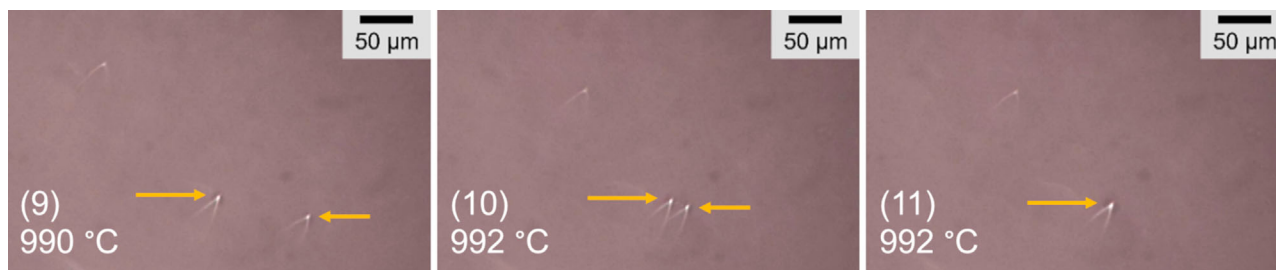


FIGURE 7 Coalescence of two silver drops (orange arrows) in the Ag0.01NZN-B melt. The silver drops, moving within the glass melt (9), approached one another (10) and coalesced into a single silver drop (11)

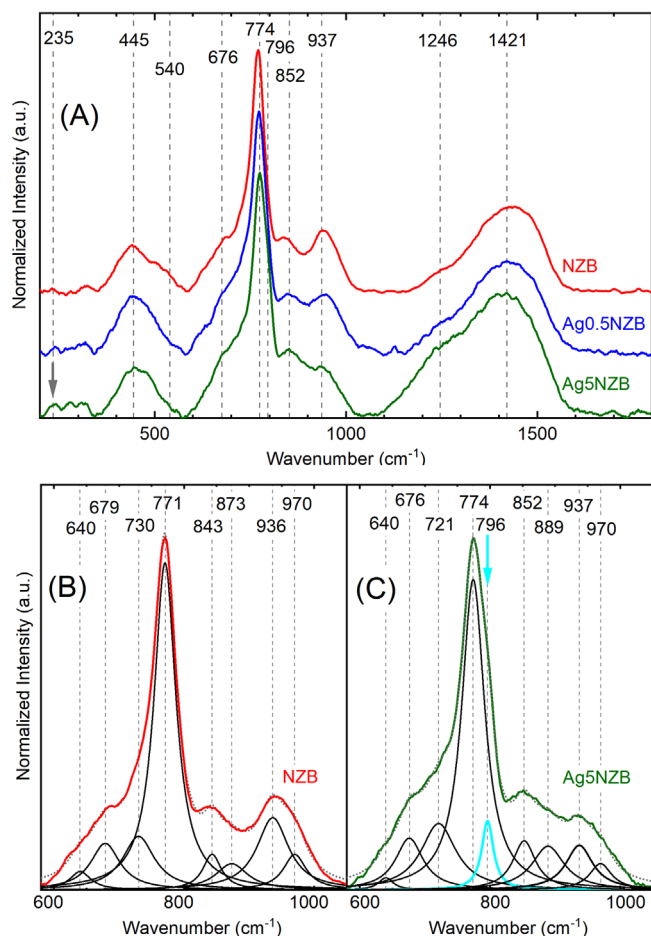


FIGURE 8 Raman spectra of NZB,²⁶ Ag0.5NZB, and Ag5NZB glasses (A). All curves were baseline corrected, normalized with respect to their maximum intensity at ≈ 770 cm^{-1} , and staggered for better clarity. Deconvoluted Lorentz profiles between 580 and 1050 cm^{-1} for NZB (B) and Ag5NZB (C)

For the ternary borate system, glass formation was received by Anavekar et al.⁴⁷, as well as Gowda and Anavekar⁴⁸ for up to ~ 30 mol% ($\text{Na}_2\text{O} + \text{ZnO}$) without silver. In the system $x\text{Na}_2\text{O} - (20-x)\text{Ag}_2\text{O} - 80\text{B}_2\text{O}_3$ with $x = 1, 10, 19$ mol%, Boulos and Kreidl⁴⁹ also proved glass for-

mation. Later, van Gemert et al.⁵⁰, Matusita et al.⁵¹, and Sharma et al.⁵² reported about glass formation in $\text{Na}_2\text{O} - \text{Ag}_2\text{O} - \text{B}_2\text{O}_3$ up to 30 mol% ($\text{Ag}_2\text{O} + \text{Na}_2\text{O}$). The Ag_2O solubility increases with decreasing Na_2O content.^{53,54} Wakasugi et al.⁵⁴ could dissolve 5 mol% Ag_2O in $5\text{Ag}_2\text{O} - 22\text{Na}_2\text{O} - 73\text{B}_2\text{O}_3$ (mol%) molten at 1150 °C. Much higher silver dissolution was possible without Na_2O in $23\text{Ag}_2\text{O} - 51\text{B}_2\text{O}_3 - 26\text{Al}_2\text{O}_3$ (mol%) molten at 1150 °C.⁵⁴ The decrease of silver dissolution with increasing sodium content is explained by Maekawa et al.⁵³ to be caused by the lower basicity of silver oxide compared to that of sodium oxide.

The trend that silver solubility decreases with increasing sodium content is consistent with the Ag/Zn-peak area ratios extracted from Figure 3 as Ag5NZB contains ~ 4.5 mol% less sodium than Ag0.5NZB. Presence of the Ag–O band at 235 cm^{-1} of Figure 8 also supports this result. Figures 2 and 5 clearly indicate limited silver dissolution < 0.5 mol% in the paste glass under study. Figure 7 reveals the precipitation of silver drops even in the glass Ag0.01NZN-B indicating a dissolution limit < 0.01 mol% Ag_2O . Thus, dissolution of up to 5 mol% Ag_2O into the $\text{Na}_2\text{O} - \text{ZnO} - \text{B}_2\text{O}_3$ glasses, as expected from consideration of the glass forming limit in the systems $\text{Na}_2\text{O} - \text{B}_2\text{O}_3$ ³⁷ and $\text{ZnO} - \text{B}_2\text{O}_3$ ⁵⁵ (Figure 9), was not achieved.

The simultaneous presence of atomic and ionic silver species is expected to be due to reactions (1) and (2) taking place during heating of all batches studied. Metallic silver is predicted as the decomposition of silver nitrate becomes significant around 250 °C⁵⁶ and is finished at 440 °C.^{30,56,57} Thus, solid nonregularly shaped metallic silver particles at $T < 962$ °C (see Figures 4 and 5) were traced back to the following Equation (1):



Jiménez et al.⁵⁸ and Simo et al.⁵⁹ showed that metallic silver has to be oxidized again to be incorporated as Ag^+ into the glassy network. Then, for the presence of Ag^+ in

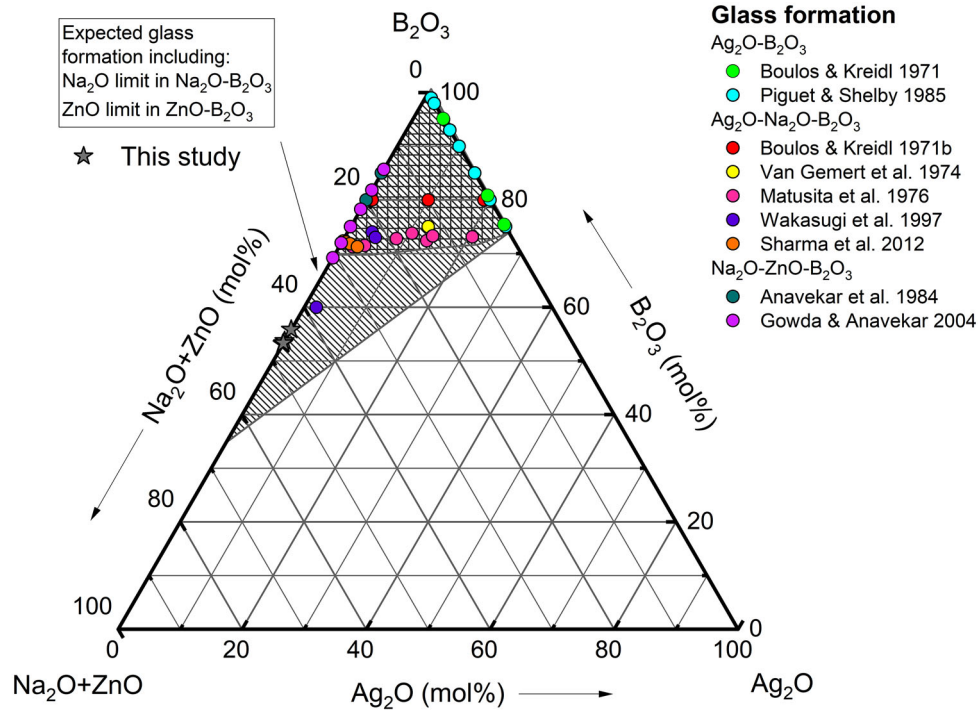
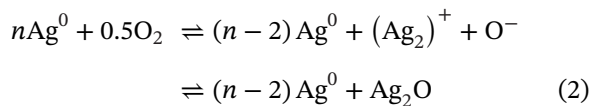


FIGURE 9 Pseudoternary $\text{Ag}_2\text{O}-(\text{Na}_2\text{O}+\text{ZnO})-\text{B}_2\text{O}_3$ system. Obtained composition of glasses prepared for this study (gray star) and those of homogeneous glasses reported in the binary $\text{Ag}_2\text{O}-\text{B}_2\text{O}_3$ system (Boulos and Kreidl 1971²¹, Piguët and Shelby 1985⁴⁶), the ternary $\text{Ag}_2\text{O}-\text{Na}_2\text{O}-\text{B}_2\text{O}_3$ system (Boulos and Kreidl 1971b⁴⁹, van Gemert et al. 1974⁵⁰, Matusita et al. 1976⁵¹, Wakasugi et al. 1997⁵⁴ and Sharma et al. 2012⁵²), and the ternary $\text{Na}_2\text{O}-\text{ZnO}-\text{B}_2\text{O}_3$ system (Anavekar et al. 1984⁴⁷, Gowda and Anavekar 2004⁴⁸); expected glass formation includes Na_2O limit in the $\text{Na}_2\text{O}-\text{B}_2\text{O}_3$ ³⁷ and ZnO limit in the $\text{ZnO}-\text{B}_2\text{O}_3$ ⁵⁵ systems, respectively

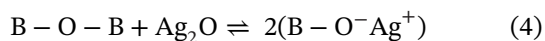
the studied glasses one has



Equation (2) points out that dissolution of silver as Ag^+ depends on the availability of oxygen.⁵³

Silver ions are expected to act in borate glasses as network-modifying alkali ions.^{21,60} Thereby, Ag^+ similar to Na^+ will balance the charge of $[\text{B}\text{O}_4]^-$ -units according to Equation (3) in binary borate glasses of up to 30 mol% Ag_2O and saturate the charge of NBOs as per Equation (4) for higher Ag_2O fractions.^{37,45}

Minor amounts of NBOs were shown in binary alkali and silver borate glasses already beginning with a content of 15 mol% network modifier.⁶⁰



In Zn-borate glasses, Zn^{2+} similar to Mg^{2+} preferably compensates the negative charge of units with a high number of NBOs, such as pyroborate.⁶¹ Due to the sufficiently high and constant amounts of zinc ions in the prepared glasses, respective borate groups with NBOs are still found

in $\text{Ag}5\text{N}Z\text{B}$. Additionally, the formation of ZnO_4 is possible, and respective Raman bands were observed in the spectra for all samples under study here. The resulting structural changes indicate a decrease of $[\text{B}\text{O}_4]^-$ units and an increase of BO_3 units with decreasing Na^+ content and metallic silver precipitation. If the silver would not precipitate, the percentage of modifier ions would be comparable for all glasses under consideration here. As sodium carbonate was replaced by silver nitrate in the batches and silver precipitated, the total amount of network modifiers decreases from $\text{Ag}0.5\text{N}Z\text{B}$ to $\text{Ag}5\text{N}Z\text{B}$. Thus, less $\text{Na}^+ + \text{Ag}^+$ is available for charge compensation to form $[\text{B}\text{O}_4]^-$ groups in $\text{Ag}5\text{N}Z\text{B}$. This effect is seen in Figure 8, where the band at 937 cm^{-1} assigned to $[\text{B}\text{O}_4]^-$ -units decreases in intensity from $\text{Ag}0.5\text{N}Z\text{B}$ to $\text{Ag}5\text{N}Z\text{B}$. For the same reason, the weak band of boroxol rings^{37-39,41} newly appears in $\text{Ag}5\text{N}Z\text{B}$ at 796 cm^{-1} (Figure 8C, cyan curve). Boroxol rings were not detected in $\text{N}Z\text{B}$ and $\text{Ag}0.5\text{N}Z\text{B}$ due to the higher amounts of Na^+ .

4.2 | Silver precipitation

Mobility of the Ag^0 particles or droplets depends on the viscosity of the melt. In a separate study,⁶² viscosity data

were determined for the sodium–zinc–borate glass under consideration here. A MYEGA-fit of those data results in an extrapolated viscosity range of $\log \eta$ (η in Pa s) ~ -0.5 to -0.9 in the temperature range between 950 and 1050°C.⁶² This allows the high convective motion of the melt.

The observed coalescence of silver droplets is driven by the reduction of the total free surface enthalpy of the system⁶³ and is probably affected by an interplay of the Stokes motion, convective flow, and the Marangoni convection. Pronounced Stokes motion is expected due to the three to four times higher density of liquid silver droplets, whereas convective flow of the liquid matrix forces the embedded droplets to follow complex patterns of motion. In the case of the Marangoni convection, the motion of droplets is additionally affected by compositional or temperature differences of interfacial energy.⁶³ In general, convection will accelerate the matter transport at $T > 962^\circ\text{C}$ as both silver droplets and borate matrix are in the liquid state. However, coarsening of the droplet population was not observed, although a diffusive transport of silver from smaller to larger droplets should proceed in the samples. On the one hand, the lack of ripening probably originates from the relative large distance between individual droplets and their low number, which did not reach statistical significance. On the other hand, repetitive size measurements were hindered due to their relative fast lateral movement but also due to rapid submerging out of the focus area of the HSM. Moreover, due to the small amount of dissolved silver in the borate liquid, re-precipitation of Ag^+ during cooling down in the HSM was not observed (see Figure 6).

5 | CONCLUSIONS

Most of the batched Ag^+ of AgNO_3 was reduced to metallic silver and formed droplets (diameter < 3 mm) in glass ingots after melt-quenching. A silver dissolution limit (< 0.01 mol% Ag_2O) in the studied glasses was approximated from HSM experiments. In turn, the precipitation of metallic silver shifted the composition of the glass from the target so that Raman spectra indicated an increase of BO_3 units at the expense of $[\text{BO}_4]^-$ units in the glass matrix.

Using HSM, metallic Ag^0 precipitation was observed in situ in heated raw material batches or mixtures of glass frit and AgNO_3 . Before the borate glass fully liquified, the used AgNO_3 liberated metallic silver and formed clustered aggregates, which in turn liquified to droplets above the Ag melting point. Smaller droplets of liquid silver ($d < \sim 20$ μm) showed a stepwise growth by coalescence with other ones in the low viscous melt, whereas larger droplets remain constant in

size during subsequent dwelling and cooling to glass transition.

AUTHOR CONTRIBUTION

Lina Heuser: leader, experimentation, analysis, design, writing, and revision. Marianne Nofz: contributor, advisor, design, writing, and revision. Joachim Deubener: advisor, academic support, writing, and approval. Ralf Müller: advisor, third-party funding acquisition, writing, and approval.

ACKNOWLEDGMENTS

The financial support of the Deutsche Forschungsgemeinschaft (DFG) in the research project MU 963/17-1 is gratefully acknowledged. The authors sincerely thank M. Buchheim, Q. H. Le, and W. Mohring for EDX measurements, T. Schmid for the helpful instruction in Raman spectroscopy, and M. Roßmüller-Felz for assistance with hot-stage microscopy.


Open access funding enabled and organized by Projekt DEAL.

ORCID

Lina Heuser  <https://orcid.org/0000-0001-9151-1508>

Marianne Nofz  <https://orcid.org/0000-0002-5629-092X>

Ralf Müller  <https://orcid.org/0000-0002-1044-2035>

Joachim Deubener  <https://orcid.org/0000-0002-3474-7490>

REFERENCES

- Adams D, Alford TL, Mayer JW. Silver metallization: stability and reliability. Derby B, editor. London: Springer Verlag London; 2008.
- Cheek GC, Mertens RP, Van Overstraeten R, Frisson L. Thick-film metallization for solar cell applications. *IEEE Trans Electron Devices*. 1984;31(5):602–9.
- Rane S, Khanna P, Seth T, Phatak G, Amalnerkar D, Das B. Firing and processing effects on microstructure of fritted silver thick film electrode materials for solar cells. *Mater Chem Phys*. 2003;82(1):237–45.
- Ballif C, Huljić D, Willeke G, Hessler-Wyser A. Silver thick-film contacts on highly doped n-type silicon emitters: structural and electronic properties of the interface. *Appl Phys Lett*. 2003;82(12):1878–80.
- Hong K-K, Cho S-B, You JS, Jeong J-W, Bea S-M, Huh J-Y. Mechanism for the formation of Ag crystallites in the Ag thick-film contacts of crystalline Si solar cells. *Sol Energy Mater Sol Cells*. 2009;93(6–7):898–904.
- Yata K, Yamaguchi T. Ostwald ripening of silver in glass. *J Mater Sci*. 1992;27(1):101–6.
- Verband Deutscher Maschinen- und Anlagenbau (VDMA Photovoltaic Equipment). International Technology Roadmap for Photovoltaic (ITRPV). 2018 Results, Tenth Edition; 2019 [cited 2021 October 4]. Available from: <https://pv-manufacturing.org/wp-content/uploads/2019/03/ITRPV-2019.pdf>

8. Yang W, Sun Q, Lei Q, Zhu W, Li Y, Wei J, et al. Formation of a highly conductive thick film by low-temperature sintering of silver paste containing a $\text{Bi}_2\text{O}_3\text{-B}_2\text{O}_3\text{-ZnO}$ glass frit. *J Mater Process Technol.* 2019;267:61–7.
9. Körner S, Eberstein M. Inventors; Fraunhofer-Gesellschaft zur Förderung der angewandten Forschung, assignee. Method for producing a silver-containing glass powder, and use of the glass powder. Patent WO2016062820A1. 2016.
10. Koo HY, Kim JH, Ko YN, Jung DS, Kang YC. Preparation of silver–glass composite powder and conducting film. *J Ceram Soc Jpn.* 2010;118(1377):353–6.
11. Kim JH, Koo HY, Ko YN, Kang YC. Characteristics of Bi-based glass frit having similar mean size and morphology to those of silver powders at high firing temperatures. *J Alloys Compd.* 2010;497(1–2):259–66.
12. Jean JH, Chang CR, Lei CD. Sintering of a crystallizable $\text{CaO-B}_2\text{O}_3\text{-SiO}_2$ glass with silver. *J Am Ceram Soc.* 2004;87(7):1244–9.
13. Körner S. Lösungs- und Ausscheidungsprozesse in silberhaltigen Glasschmelzen bei der thermischen Kontaktierung von multikristallinem Silicium [dissertation]. Dresden: Technische Universität Dresden; 2018.
14. Eberstein M, Rabe T, Schiller W. Influences of the glass phase on densification, microstructure, and properties of low-temperature co-fired ceramics. *Int J Appl Ceram Technol.* 2006;3:428–36.
15. Yao S, Xing J, Zhang J, Xiong S, Yang Y, Yuan X, et al. Microscopic investigation on sintering mechanism of electronic silver paste and its effect on electrical conductivity of sintered electrodes. *J Mater Sci Mater Electron.* 2018;29(21):18540–6.
16. Chung YS, Kim H-G. Effect of the oxide glass on the metal sintering behavior in silver thick-film system. In: Proceedings of the Korean Ceramic Society Conference. The Korean Ceramic Society; 1986.
17. Reinhardt K, Schmidt U, Körner S, Jurk R, Partsch U, Eberstein M. Observation of the contact formation of PV frontside pastes by in-situ contact resistance measurement. *Energy Procedia.* 2014;55:702–7.
18. Qin J, Zhang W, Bai S, Liu Z. Study on the sintering and contact formation process of silver front side metallization pastes for crystalline silicon solar cells. *Appl Surf Sci.* 2016;376:52–61.
19. Eberstein M, Schmidt U, Körner S, Reinhardt K, Jurk R, Partsch U. In-situ observations of glass frit related effects during the front side paste contact formation. In: Abbott D, editor. 2014 IEEE 40th Photovoltaic Specialist Conference (PVSC). Denver, USA: IEEE; 2014. p. 3463–9.
20. Borsella E, Battaglin G, Garcia MA, Gonella F, Mazzoldi P, Polloni R, et al. Structural incorporation of silver in sodalime glass by the ion-exchange process: a photoluminescence spectroscopy study. *Appl Phys A.* 2000;71(2):125–32.
21. Boulos EN, Kreidl N. Structure and properties of silver borate glasses. *J Am Ceram Soc.* 1971;54(8):368–75.
22. Duffy JA, Harris B, Kamitsos EI, Chryssikos GD, Kapoutsis JA. Polarising power and polarisability of the Ag^+ ion in glass: the basicity of silver (I) oxide. *Phys Chem Glasses.* 1998;39(5):275–80.
23. Chen X, Zhao J, Xu X, Ren K, Luo X, Sun X, et al. Phase separation strategy to facilitate form fluorescent $[\text{Ag}_2]^{2+}/[\text{Ag}_m]^{n+}$ quantum clusters in boro-alumino-silicate multiphase glasses. *Phys Chem Chem Phys.* 2018;20(37):23942–7.
24. Wakasugi T, Ohkawa A, Fukunaga J, Ota R. Solubility of Ag_2O in the $\text{B}_2\text{O}_3\text{-Al}_2\text{O}_3$ system. *J Non-Cryst Solids.* 1999;255(2–3):127–31.
25. Deutsches Institut für Normung e.V. DIN 51086-2. Prüfung von oxidischen Roh- und Werkstoffen für Keramik, Glas und Glasuren, Teil 2: Bestimmung von Ag, As, B, Ba, Be, Bi, Ca, Cd, Ce, Co, Cr, Cu, Er, Eu, Fe, La, Mg, Mn, Mo, Nd, Ni, P, Pb, Pr, S, Sb, Se, Sn, Sr, Ti, V, W, Y, Yb, Zn, Zr durch optische Emissionsspektrometrie mit induktiv gekoppeltem Plasma (ICP OES). Berlin; 2004.
26. Heuser L, Nofz M. Alkali and alkaline earth zinc and lead borate glasses: structure and properties. *J Non-Cryst Solids.* 2022;15:100109.
27. OriginLab Corporation. Origin, Version 2020. Northampton, MA, USA: OriginLab Corporation; 2020.
28. Wang X, Fan X-g, Xu Y-j, Wang X-f, He H, Zuo Y. A baseline correction algorithm for Raman spectroscopy by adaptive knots B-spline. *Meas Sci Technol.* 2015;26(11):115503.
29. Schmid T, Jungnickel R, Dariz P. Raman band widths of anhydrite II reveal the burning history of high-fired medieval gypsum mortars. *J Raman Spectrosc.* 2019;50(8):1154–68.
30. Sitzmann H. Silberniträt in RÖMPP [Online]. Stuttgart: Georg Thieme Verlag; 2010. [Cited 2021 October 05]. Available from: <https://roempp.thieme.de/lexicon/RD-19-02404>
31. Sitzmann H. Silber in RÖMPP [Online]. Stuttgart: Georg Thieme Verlag; 2007. [Cited 2021 Oct 05]. Available from: <https://roempp.thieme.de/lexicon/RD-19-02382>
32. Kirshenbaum A, Cahill J, Grosse A. The density of liquid silver from its melting point to its normal boiling point 2450 K. *J Inorg Nucl Chem.* 1962;24(3):333–6.
33. Martina I, Wiesinger R, Jembrih-Simbürger D, Schreiner M. Micro-Raman characterisation of silver corrosion products: instrumental set up and reference database. *E-Preserv Sci.* 2012;9:1–8.
34. Bettinelli M, Speghini A, Ferrari M, Montagna M. Spectroscopic investigation of zinc borate glasses doped with trivalent europium ions. *J Non-Cryst Solids.* 1996;201(3):211–21.
35. Yadav AK, Singh P. A review of the structures of oxide glasses by Raman spectroscopy. *RSC Adv.* 2015;5(83):67583–609.
36. Kamitsos EI, Karakassides MA, Chryssikos GD. Structure of borate glasses. Part I. Raman study of caesium, rubidium, and potassium borate glasses. *Phys Chem Glasses.* 1989;30(6):229–34.
37. Kamitsos EI, Chryssikos GD. Borate glass structure by Raman and infrared spectroscopies. *J Mol Struct.* 1991;247:1–16.
38. Brill TW. Raman spectroscopy of crystalline and vitreous borates. [PhD Thesis]. Eindhoven: Technische Hogeschool Eindhoven; 1976.
39. Konijnendijk WL, Stevels JM. The structure of borate glasses studied by Raman scattering. *J Non-Cryst Solids.* 1975;18(3):307–31.
40. Othman HA, Herrmann A, Möncke D. Mixed barium-lead borate glasses studied by optical and vibrational spectroscopy. *Int J Appl Glass Sci.* 2019;10(3):339–48.
41. Yao ZY, Möncke D, Kamitsos EI, Houizot P, Célarié F, Rouxel T, et al. Structure and mechanical properties of copper-lead and copper-zinc borate glasses. *J Non-Cryst Solids.* 2016;435:55–68.
42. Maniu D, Iliescu T, Ardelean I, Cinta-Pinzaru S, Tarcea N, Kiefer W. Raman study on $\text{B}_2\text{O}_3\text{-CaO}$ glasses. *J Mol Struct.* 2003;651:485–8.

43. Konijnendijk WL. The structure of borosilicate glasses. Philips Research Reports Supplements 1975, No.1. [PhD Thesis]. Eindhoven: Technological University Eindhoven; 1975.
44. Kamitsos EI, Karakassides MA, Chryssikos GD. Vibrational spectra of magnesium-sodium-borate glasses. 2. Raman and mid-infrared investigation of the network structure. *J Phys Chem.* 1987;91(5):1073–9.
45. Chryssikos GD, Kamitsos EI, Karakassides MA. Structure of borate glasses. Part 2. Alkali induced network modifications in terms of structure and properties. *Phys Chem Glasses.* 1990;31(3):109–16.
46. Piguet JL, Shelby JE. Preparation and properties of silver borate glasses. *J Am Ceram Soc.* 1985;68(8):450–5.
47. Anavekar RV, Devaraj N, Ramakrishna J. DC electrical conductivity of $\text{Na}_2\text{O-ZnO-B}_2\text{O}_3$ glass system. *Bull Mater Sci.* 1984;6:1009–12.
48. Gowda VCV, Anavekar RV. Elastic properties and spectroscopic studies of $\text{Na}_2\text{O-ZnO-B}_2\text{O}_3$ glass system. *Bull Mater Sci.* 2004;27(2):199–205.
49. Boulos E, Kreidl N. Mixed-cation effect in silver borate glasses. *J Am Ceram Soc.* 1971;54(6):318–9.
50. van Gemert WJT, Van Ass HMJM, Stevels JM. Internal friction and dielectric losses of mixed alkali borate glasses. *J Non-Cryst Solids.* 1974;16(2):281–93.
51. Matusita K, Ito M, Kamiya K, Sakka S. The electric conduction in mixed cation glasses of the $\text{Ag}_2\text{O-Na}_2\text{O-B}_2\text{O}_3$ system. *Yogyo-Kyokai-Shi.* 1976;84(10):496–508.
52. Sharma V, Singh SP, Mudahar GS, Thind KS. Synthesis and optical characterization of silver doped sodium borate glasses. *New J Glass Ceram.* 2012;2(4):133–7.
53. Maekawa T, Yokokawa T, Niwa K. Solubility of Ag_2O in $\text{Na}_2\text{O-B}_2\text{O}_3$ melts. *Bull Chem Soc Jpn.* 1969;42(3):677–81.
54. Wakasugi T, Hirota A, Fukunaga J, Ota R. Solubility of Ag_2O into the $\text{Na}_2\text{O-B}_2\text{O}_3\text{-Al}_2\text{O}_3$ system. *J Non-Cryst Solids.* 1997;210(2–3):141–7.
55. Azooz MA, ElBatal HA. Preparation and characterization of invert $\text{ZnO-B}_2\text{O}_3$ glasses and its shielding behavior towards gamma irradiation. *Mater Chem Phys.* 2020;240:122129.
56. Lara HH, Romero-Urbina DG, Pierce C, Lopez-Ribot JL, Arellano-Jiménez MJ, Jose-Yacaman M. Effect of silver nanoparticles on *Candida albicans* biofilms: an ultrastructural study. *J Nanobiotechnol.* 2015;13(1):1–12.
57. Kwon J-W, Yoon S-H, Lee S-S, Seo K-W, Shim I-W. Preparation of silver nanoparticles in cellulose acetate polymer and the reaction chemistry of silver complexes in the polymer. *Bull Korean Chem Soc.* 2005;26(5):837–40.
58. Jiménez J, Sendova M, Hartsfield T, Sendova-Vassileva M. In situ optical microspectroscopy of the growth and oxidation of silver nanoparticles in silica thin films on soda-lime glass. *Mater Res Bull.* 2011;46(2):158–65.
59. Simo A, Polte J, Pfänder N, Vainio U, Emmerling F, Rademann K. Formation mechanism of silver nanoparticles stabilized in glassy matrices. *J Am Chem Soc.* 2012;134(45):18824–33.
60. Kapoutsis JA, Kamitsos EI, Chryssikos GD. A structural study of silver borate glasses by infrared reflectance and Raman spectroscopies. In: Wright AC, Feller SA, Hannon AC, editors. *Proc Second Int Conf on Borates Glasses, Crystals and Melts.* 1997. p. 303–12.
61. Möncke D, Kamitsos EI, Palles D, Limbach R, Winterstein-Beckmann A, Honma T, et al. Transition and post-transition metal ions in borate glasses: borate ligand speciation, cluster formation, and their effect on glass transition and mechanical properties. *J Chem Phys.* 2016;145(12):124501.
62. Heuser L, Nofz M, Müller R. Alkali and alkaline earth zinc and lead borate glasses: sintering and crystallization. *J Non-Cryst Solids.* 2022;15:100116.
63. Ratke L, Thieringer WK. The influence of particle motion on Ostwald ripening in liquids. *Acta Metall.* 1985;33(10):1793–802.

SUPPORTING INFORMATION

Additional supporting information can be found online in the Supporting Information section at the end of this article.

How to cite this article: Heuser L, Nofz M, Müller R, Deubener J. Silver dissolution and precipitation in an $\text{Na}_2\text{O-ZnO-B}_2\text{O}_3$ metallization paste glass. *Int J Appl Glass Sci.* 2022;1–11.
<https://doi.org/10.1111/ijag.16613>